Transition metal qubits in 4*H*-silicon carbide: A correlated EPR and DFT study of the spin $S = 1$ vanadium V^{3+} center

H. J. von Bardeleben,[1] S. A. Zargaleh,[2] J. L. Cantin,[1] W. B. Gao,[2] T. Biktagirov,[3] and U. Gerstmann[3]

[1]*Sorbonne Université, Institut des Nanosciences de Paris (INSP), UMR 7588 au CNRS 4 place Jussieu, 75005 Paris, France*

[2]*Division of Physics and Applied Physics, School of Physical and Mathematical Sciences, Nanyang Technological University, Singapore 637371, Singapore*

[3]*Department of Physics, University of Paderborn, Warburger Straße 100, 33098 Paderborn, Germany*

(Received 8 October 2019; published 30 December 2019)

Whereas intrinsic defects in silicon carbide (SiC) have been widely considered for qubit applications, transition metals in this material have not yet been recognized as alternative systems. We have investigated the magneto-optical properties of the V^{3+} center in 4*H*-SiC by electron paramagnetic resonance (EPR) and photo-EPR spectroscopy in view of their possible application in quantum technology. We show that they fulfill all the requirements for such applications: a high-spin $S = 1$ ground state, optically induced ground-state spin polarization of more than 70%, long spin-lattice relaxation times of the order of a second, as well as associated zero-phonon photoluminescence emission lines in the range of 1.8 μm. Further, the zero-field splitting parameter D is temperature dependent and increases between $T = 4$ K and $T = 292$ K linearly with a rate of 440 kHz/K, allowing potential nanoscale temperature sensing. These properties make the vanadium acceptor an extremely promising candidate for qubit applications with optical properties in the telecommunication optical range.

DOI: 10.1103/PhysRevMaterials.3.124605

I. INTRODUCTION

Solid-state spins are currently considered and used for realizing different applications in quantum technology [1,2]. These applications are based on the particular optical and magnetic properties of the solid-state qubits; preferably, they should also be hosted in standard microelectronics materials such as silicon, silicon carbide, or III-V semiconductor compounds. The latter property is a requirement for scaling and interconnection of qubits on electronic chips. The most established case of a solid-state qubit is the negatively charged nitrogen-vacancy (NV) center in diamond, a three-level system with a spin $S = 1$ ground state, a spin $S = 1$ excited state, giving rise to a radiative recombination with narrow zero-phonon lines (ZPL) and intermediate singlet states, which due to spin-dependent recombination rates polarize the spin of the ground state in the $m_s = 0$ level [Fig. 1(a)]. The presence of one or multiple singlet state(s) is a key property, allowing optically induced ground-state spin polarization and optical initialization. For a detailed review of the NV center in diamond, see, e.g., Ref. [3]. It has been studied in large ensembles in bulk crystals and as a single defect in nanodiamonds. The NV center is an associated defect of a carbon vacancy and a nitrogen neighbor, which only in the negative (1-) charge state has the required properties. Even though its exceptional magneto-optical properties have allowed major achievements [3–6], this system presents nevertheless some drawbacks for applications. First the associated optical range: the principal photoluminescence ZPL is at 632 nm, a wavelength not suitable for long-distance transmission in optical fibers. Further, the NV center formation requires an irradiation and thermal annealing process which renders a precise localization and spatial distribution of these centers difficult, and the last diamond is not compatible with standard microelectronic materials.

More recently, silicon carbide (SiC) has been proposed as a promising alternative host for defects with potentially similar applications [7–11]. The use of SiC would relieve some of the drawbacks mentioned above, with in particular the shift of the optical properties from the visible to the near infrared [Fig. 1(b)]. Since then, many of these predictions have been confirmed for several defect centers. The defect centers with demonstrated properties for QT applications are the Si monovacancies (V_{Si}) in the negative charge state [12–14], the divacancies ($V_{Si}V_C$) in the neutral charge state [15,16], and the NV centers ($V_{Si}N_C$) in the 1- charge state [17–22]. Their basic properties are compared in Table I. All these centers have high-spin ground states with spin $S = 3/2(V_{Si}^-)$ or spin $S = 1(V_{Si}V_C{}^0, NV^-)$, respectively. They show, however, major differences in their optical spectral range and symmetry properties: the spectral range, determined by the lowest radiative recombination, ranges from 850 nm ($V_{Si}{}^-$) to 1300 nm (NV^-). The hexagonal SiC polytypes introduce also new functionalities due to the lower symmetry of their crystal structure: the nonequivalence of the lattice sites (hexagonal, quasicubic) introduces multiple centers with similar but distinct properties. It gives further rise to so-called *axial* and *basal* configurations of pair centers (e.g., VV, NV). The unique orientation of the axial centers with the defect axis parallel the crystal c axis is a useful property for magnetic field sensing applications. The cubic polytype of SiC, on the other hand, can be efficiently epitaxied on silicon substrates, which should allow scaling and interconnection with standard silicon technology.

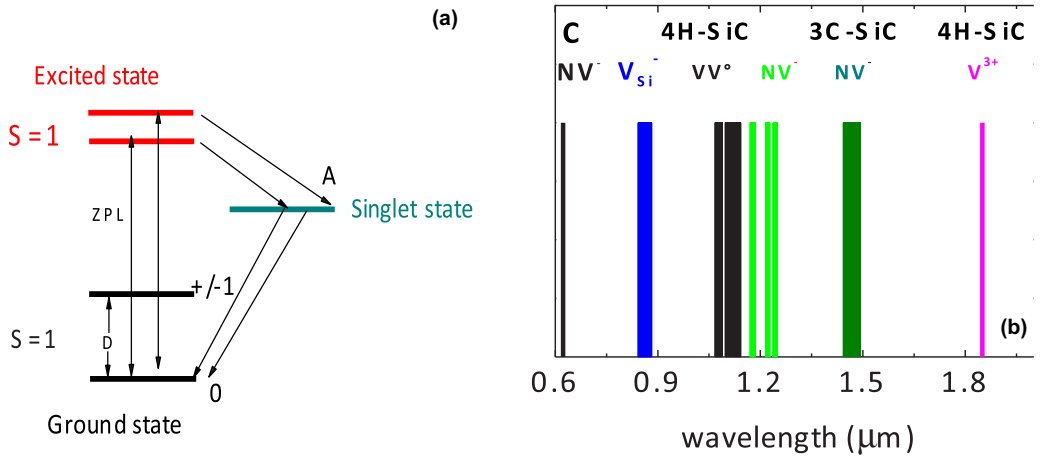

FIG. 1. (a) Level scheme of spin $S = 1$ qubits such as NV centers in SiC. (b) Spectral range of intracenter ZPL emission lines of NV centers in diamond, silicon monovacancies, divacancies, NV centers in 4*H* and 3C-SiC, and vanadium acceptors [32] in 4*H*-SiC.

Very recently, transition metals in SiC have also been proposed as candidates for QT applications [23–25]. They are in general deep centers with often radiative intracenter transitions in the near infrared close to the telecommunication spectral range of 1.5 μm. But the knowledge of their magneto-optical properties in SiC is still very incomplete or most often absent. Among the transition metals vanadium has been particularly well studied in 4*H* and 6*H*-SiC some decades ago for its use in microelectronic applications, e.g., vanadium doping in the 10^{18} cm^{-3} concentration range, allowed to obtain highly resistive semi-insulating substrates by compensating residual donor and acceptor impurities [26–32]. As nowadays such substrates can be made with the use of intrinsic defects, generated under nonstoichiometric growth conditions, the research interest for this dopant has strongly diminished. The early studies performed some 20 years ago have established that vanadium in 4*H*-SiC as well as in 6*H*-SiC is an amphoteric deep center with three stable charge states V^{3+}, V^{4+}, V^{5+} and charge transition levels at E_{CB}–1.6 eV and E_{CB}–0.8 eV, respectively. In two charge states vanadium has nonzero spin ground states (3+ with $S = 1$, 4+ with $S = 1/2$), whereas V^{5+} is diamagnetic ($S = 0$).

In this work we show that vanadium in the spin-triplet ($S = 1$) acceptor state V^{3+} in 4*H*-SiC has interesting properties, which might allow applications in quantum technology. In particular, its optical properties are still further shifted in the infrared as compared to the $N_C V_{Si}$ centers, for example. In principle, its orbital singlet $^3A_2$ ground state with a spin $S = 1$ should give rise to long spin-lattice relaxation times and weak electron-phonon coupling with consequently strong ZPL emission. The high nuclear spin $I = 7/2$ of its principal isotope ^{51}V is an additional interesting property for polarization transfer from the electron spin to the nuclear spin system, a resource for quantum memories. Due to the lower symmetry of the 4*H*-SiC as compared to diamond, the cation lattice sites are no longer equivalent. In 4*H*-SiC we have two distinct lattice sites, labeled quasicubic (k) and hexagonal (h), and Si site substituted vanadium introduces two distinct centers $V(h)$, $V(k)$, with different magnetic and optical properties. The magneto-optical properties of the V^{3+} acceptors $V^{3+}(h, k)$ have been only marginally investigated. Even their charge transition levels are controversially discussed; they are known to be somewhere deep in the 0.8 eV … 1.2 eV range below the conduction band [26–28,31,32]. Very recently, the optical properties of the donor state V^{4+} ($S = 1/2$) have been investigated. Showing an optical emission at 1.3 μm, it has been considered for application in quantum photonics [25]. In this work, we investigate the magneto-optical properties of the vanadium in the acceptor V^{3+} charge state providing a potentially more promising $S = 1$ spin-triplet ground state. We have performed *first-principles* calculations of its ground (and excited) state properties, which are further used to interpret the experimental results obtained by electron paramagnetic resonance spectroscopy (EPR).

TABLE I. Overview of electron spin, zero-field splitting parameters D and wavelength of ZPL lines of some defects with demonstrated qubit properties in 4*H*-SiC. (Here, V refers to vacancies.) The pair defects (VV and NV) give rise to four different centers each, depending on the lattice site (h, k) of their constituents; their electronic properties are similar, but distinct.

Defect	Spin S	ZFS D (GHz)	ZPL (nm)	Ref.
$V_{Si}^-(h)$	3/2	0.003	862	[33]
$V_{Si}^-(k)$	3/2	0.035	917	[33]
VV° (kk) axial	1	1.305	1132	[34]
VV° (hh) axial	1	1.336	1132	[34]
VV° (hk) *basal*	1	1.222	1108	[34]
VV° (kh) *basal*	1	1.334	1078	[34]
NV^-(kk) axial	1	1.282	1222	[17–20,22]
NV^-(hh) axial	1	1.331	1179	[17–20,22]
NV^-(hk) *basal*	1	1.193	1243	[17–20,22]
NV^-(kh) *basal*	1	1.328	1176	[17–20,22]

II. COMPUTATIONAL DETAILS

The calculations of the $^3A_2$ ground-state-spin Hamiltonian parameters and the total energy of the first excited state of the vanadium acceptors were performed within density functional theory (DFT). The defect structures were modeled with

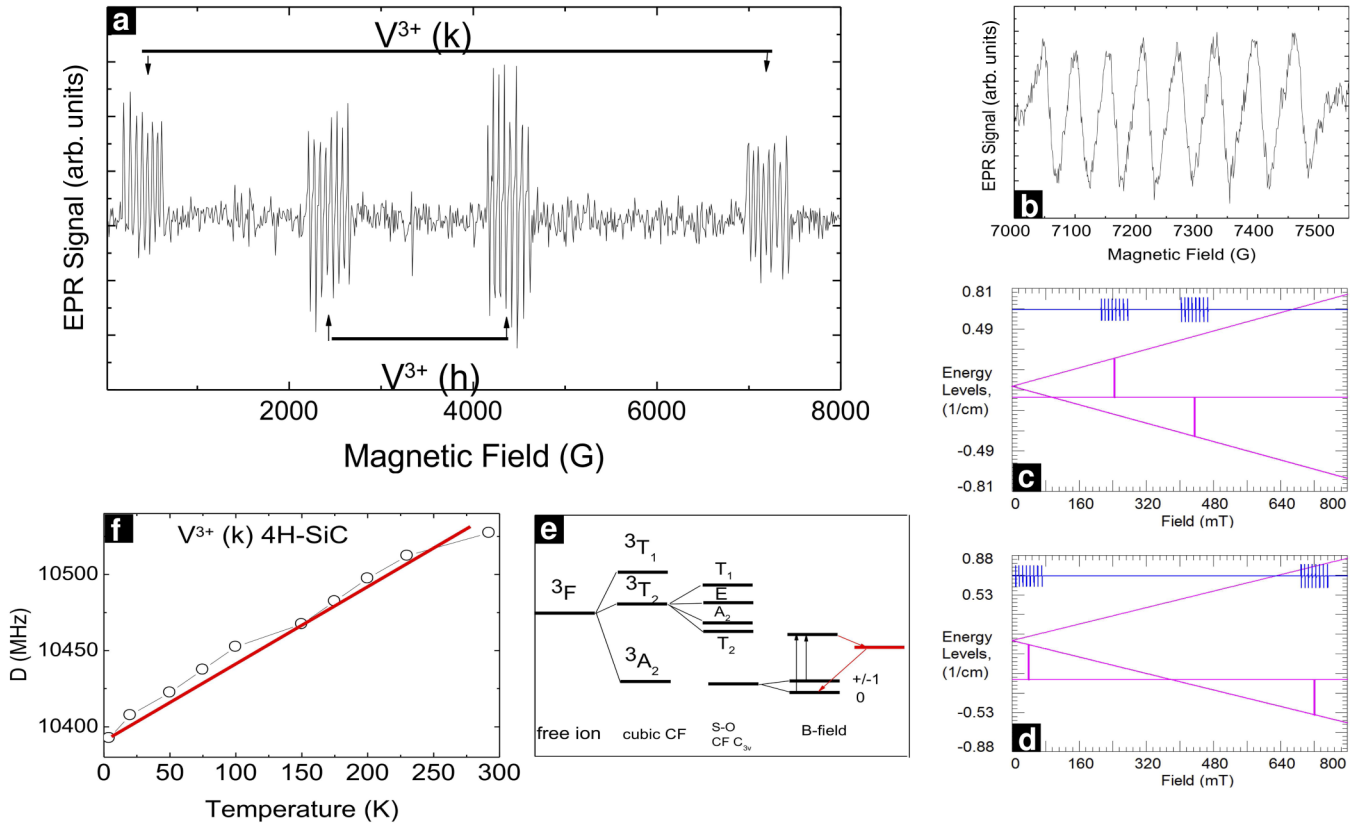

FIG. 2. (a) Low-temperature EPR spectrum of 4*H*-SiC:V showing the spectra of $V^{3+}(h)$ and $V^{3+}(k)$ for $B||c$. (b) CHF structure of the $V^{3+}(k)$ high-field line for $B||c$. (c) Energy-level scheme for the $V^{3+}(h)$ center for $B||c$, with MF frequency 9.349 GHz; the vertical lines show the resonance fields for the X-band EPR transitions. (d) Energy-level scheme for the $V^{3+}(k)$ center for $B||c$, with MW frequency 9.349 GHz. (e) Term scheme of the free-ion ^3F state of V^{3+} under the effect of the crystal field and the spin-orbit interaction. (f) $V^{3+}(k)$ zero-field splitting parameter D as a function of temperature.

hexagonal 432-atom 4*H*-SiC supercells using the QUANTUM ESPRESSO software [35,36]. The spin-spin [37] and spin-orbit [38] contributions to the zero-field splitting (ZFS), as well as the electronic g tensor and the ^{51}V hyperfine coupling constants, were calculated with the GIPAW module of QUANTUM ESPRESSO [35]. The ZPL energies were obtained with the constrained DFT approach by imposing excited occupations of the one-particle levels reflecting the $^3T_2$-like character of the excited states.

Notably, we find the spin Hamiltonian parameters of the V^{3+} center to be extremely sensitive to local distortions around the substitutional ion. Therefore, the choice of the exchange-correlation functional used for geometry optimization is crucial for reaching a reasonable accuracy with the experimental data. In particular, the Perdew-Burke-Ernzerhof (PBE) functional [39], commonly employed for defect calculation, was found to significantly underestimate the ZFS values of the V^{3+} centers. In contrast, when the defect-containing supercells were relaxed with the PBEsol functional [40], we obtained still too small but almost 2 times higher spin-orbit ZFS values. Therefore, we have used PBEsol for both geometry optimization and the magnetic and optical properties calculation, along with norm-conserving pseudopotentials and a plane-wave basis set with kinetic-energy cutoff of 90 Ry.

III. EXPERIMENTAL DETAILS

We performed electron paramagnetic resonance (EPR) and photo-EPR measurements on low-doped (10^{16} cm^{-3}) semi-insulating 4*H*-SiC:V bulk single crystals. The X-band EPR measurements were performed in the range from room temperature down to $T = 4$ K. The photo-EPR measurements and the optically induced ground-state polarization measurements were performed at $T = 4$ K. For the photoexcitation experiments we used different diode lasers with a wavelength range between 600 and 1300 nm and an output power of 30 to 100 mW. The samples were photoexcited *in situ*. The measured EPR spectra were fitted with the Visual EPR simulation tool from Grachev [41].

IV. RESULTS AND DISCUSSION

In Fig. 2(a) we show a typical low-temperature EPR spectrum. The applied magnetic field is aligned with the crystal c axis. We observe *four* groups of octet lines, which can be associated with the electronic transitions $m_s = -1 \rightarrow 0$ and $m_s = 0 \rightarrow +1$ of substitutional V^{3+} on the two lattice sites, the hexagonal (h) and (quasi-)cubic (k) [29,30]. The signature of vanadium is directly and unambiguously deduced from the resolved central hyperfine interaction [Fig. 2(b)] with a spin $I =$

TABLE II. Comparison of experimental and DFT-calculated spin Hamiltonian parameters for the V^{3+} acceptors on the (h, k) lattice sites in 4*H*-SiC: zero-field splitting parameter D, central ^{51}V hyperfine splittings $A_{||c}$, $A_{\perp c}$ (calculated isotropic Fermi contact term corrected for core polarization, thereby changing sign, not accessible in experiment) and principle values of the g tensor (slightly different from those given in Ref. [32]). DFT (PBE and PBEsol) predicted ZPL energies are also given [and belong to adiabatic transitions between the relaxed ground state and first excited state; see also Fig. 3(b)].

	g factor		ZFS			HF (^{51}V)		
	$g_{\|\|c}$	$g_{\perp c}$	D_{ss} (MHz)	D_{so} (MHz)	D_{tot} (MHz)	$A_{\|\|c}$ (MHz)	$A_{\perp c}$ (MHz)	ZPL (eV/μm)
Exp. $V^{3+}(h)$	1.951	1.956			2618	172	174	0.6691/1.853 and 0.6698/1.851
Exp. $V^{3+}(k)$	1.961	1.957			10385 (4 K) 10528 (300 K)	177	189	[32]
$V^{3+}(h)$, PBEsol	**1.9759**	**1.9765**	**52**	**1586**	**1638**	**−167**	**−166**	**0.630 1.968**
$V^{3+}(k)$, PBEsol	**1.9772**	**1.9727**	**3097**	**3077**	**6174**	**−164**	**−178**	**0.674 1.837**
$V^{3+}(h)$, PBE	1.9772	1.9776	48	823	871	−170	−167	0.747 1.675
$V^{3+}(k)$, PBE	1.9777	1.9744	2718	1790	4508	−163	−190	0.807 1.534

7/2 nucleus (with almost 100% isotopic abundance), which is a clear fingerprint of vanadium ^{51}V (I = 7/2, 99.75%). As V occupies both Si lattice sites (h, k), which have distinct electronic properties, we observe two V-related spin $S = 1$ EPR spectra. In the past the two EPR spectra have been identified with V^{3+} and associated to the cubic (k) and hexagonal (h) lattice sites, respectively [29,30]. Theoretical predictions concerning the ZFS parameter D were not available at that time, and the attribution of the EPR spectra to the (k, h) sites was based on the "*intuitive*" assumption that the h site should show the highest D value. As shown below, however, this lattice site assignment has to be revised; in the following the corrected inversed lattice site assignment will be given.

The EPR spectra of V^{3+} could be observed in the whole temperature range from $T = 4$ K to $T = 300$ K. The corresponding EPR parameters were deduced from the angular variation of their resonance fields when the magnetic field was rotated from $B||c$ to $B\perp c$. Both centers show a simple axial C_{3v} symmetry, as expected for an isolated substitutional center. The spin Hamiltonian for the axial V^{3+} spin $S = 1$ centers is given by

$$H = \mu_B H \cdot g \cdot S + D\left(S_z^2 - \tfrac{2}{3}\right) + I \cdot A \cdot S,$$

with S the electron spin, g the electron g tensor (Landé factor), which has two components $g||c$, $g\perp c$, the zero-field splitting (ZFS) parameter D, I the nuclear spin, and A the hyperfine (hf) interaction tensor of the central V nucleus.

The angular variations of the EPR spectra reveal significantly different D values of the two substitutional centers (see Table II). For the hexagonal center $V^{3+}(h)$, the numerical value of D can be directly derived from resonance fields of the spectrum for $B||c$. As for $V^{3+}(k)$ the parameter D is compatible in magnitude to the Zeeman interaction at 9 GHz; its determination requires a spectrum simulation. The principal values of the hyperfine tensor A for the interaction with the ^{51}V nucleus are obtained from the analysis of the octet structure [Fig. 2(b)]. The spin Hamiltonian parameters are in good agreement with the previously reported values obtained from EPR measurements at $T = 77$ K [30].

In Figs. 2(c) and 2(d) we show the energy-level scheme for both centers deduced from the observed spin Hamiltonian parameters. For the orientation $B||c$ we observe a level anticrossing (LAC) of the ground state at 700 G and 3000 G for $V^{3+}(h)$ and $V^{3+}(k)$, respectively, neglecting the additional substructure due to the central HF interaction. When the ground state is spin polarized at these magnetic fields, the electronic polarization will be transferred to the nuclear spin system.

The assignment of the observed V^{3+} centers to the h and k lattice sites is based on our DFT calculations. As seen from Table II, although the modulus of the PBEsol-calculated ZFS remains strongly underestimated, carefully calculated D values (including both the spin-spin and spin-orbit contributions) allow for at least a qualitative rationalization of the difference in the D values for the two centers observed in the experiment. Note that the ZFS D value depends here very sensitively on the details of the relaxation. In the cubic 3*C*-SiC polytype, the $3d^2$ occupation of the vanadium $3d$ shell results in tetrahedral symmetry and thus in a vanishing D value. In the 4*H*-SiC polytype, tiny deviations from *local* T_d symmetry result in increasing D. In any case, the V^{3+} center with the large D value has to be attributed to the quasicubic lattice site (k) and the second one with the smaller magnetic anisotropy belongs to the hexagonal lattice site (h). This can be further understood by comparing the coordination environment of the vanadium impurities: $V^{3+}(k)$ exhibits stronger axial interaction due to an additional on-axis C nearest neighbor on a hexagonal lattice site (see Fig. 3). A comparison with the past [30] shows that the attribution has to be reversed. This is also in line with recent observations [42] that in the hexagonal SiC

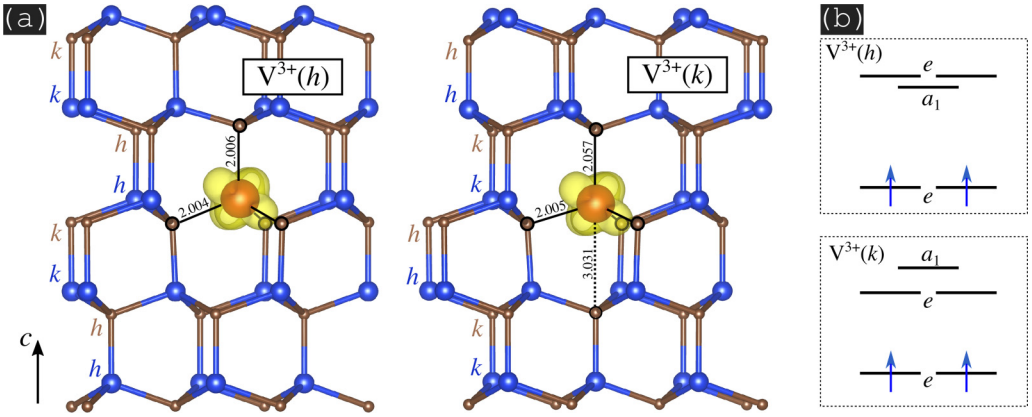

FIG. 3. (a) Details of the V^{3+} coordination environment at the h and k crystallographic sites of 4H-SiC. The presented bond lengths (in Å) to the nearest-neighbor C atoms show that $V^{3+}(h)$ exhibits almost tetrahedral geometry with minor axial distortion, whereas $V^{3+}(k)$ tends towards axially distorted, trigonal symmetry due to the presence of an additional on-axis C atom below the defect (dashed line). Yellow isosurfaces show the d-like spin-density distribution. (b) Occupations of the defect-induced single-particle levels of the vanadium 3d shell (within the band gap). Note that for $V^{3+}(h)$ and $V^{3+}(k)$ the order of the empty a_1 and e levels is reversed (in T_d symmetry belonging both to the t_2 irreducible representation).

polytypes it is the h site which mimics the high-symmetry situation in the cubic 3C-SiC material. The relation between the calculated $g_{||}$ and $g_\perp$ values [$g_{||} < g_\perp$ for $V^{3+}(h)$, and $g_{||} > g_\perp$ for $V^{3+}(k)$] is also in qualitative agreement with the experiment and provide further support for the proposed lattice site assignment.

In the case of NV centers in diamond, the variation of the ZFS parameter D with temperature can be used for temperature sensing with nanometer spatial resolution [43–45]. Even though the variation of D is small, 76 kHz/K in the range above $T = 200$ K, optically detected magnetic resonance spectroscopy of individual NV centers in nanodiamonds can measure small temperature variations of millikelvin range. However, in the low-temperature region $T < 100$ K the value of D is nearly temperature independent. We have measured by EPR the temperature dependence of the ZFS parameter D for the two V^{3+} centers [Fig. 2(f)], whereby the numerical value of D at each temperature was deduced by a simulation of the experimental spectrum for $B||c$ [41]. Within error bars of +/−15 MHz, the D value of $V^{3+}(h)$ is not temperature dependent. For the $V^{3+}(k)$ center, however, the situation is contrary. Different from the case of NV centers in diamond, the value of D of $V^{3+}(k)$ increases linearly with temperature in the full temperature range between 4 and 300 K. Such a strong variation is also different from the behavior of divacancies in 4H-SiC, for which the D value decreases with increasing temperature. The rate of increase for $V^{3+}(k)$ is 440 kHz/K, which is 6 times higher than the value reported for the NV center in diamond.

Optically induced spin polarization of the ground state, which can be read out by their associated ZPL photoluminescence line, is another key requirement for solid-state qubits. As shown schematically in Fig. 1(a) this process requires a particular excited-state-level scheme. Spin-dependent recombination, generating a ground-state spin polarization, operates via recombination through a lower-energy singlet state. Such a singlet state has not yet been observed for V^{3+} in 4H-SiC, but it has been suggested by theory [46]; these authors situate it at 0.5 eV above the ground state, resulting in a promising level scheme [see also Fig. 2(e)]. For the 4+ charge state of vanadium, the donor state with $S = 1/2$, ZPL has been reported before. The so-called (α, β) ZPL, observed at 7261 and 7700 cm^{-1} (1.377 and 1.288 μm, respectively), had been recently assigned to the $V^{4+}(h, k)$ donor states [25]. For the $S = 1$ acceptor state, however, the situation is less clear. Experimental observation of the V^{3+}-associated ZPL lines has been reported in the 1.8-μm range in both absorption and emission [30,32]. The authors observed *one* doublet ZPL at 5403 and 5397 cm^{-1} (1.851 and 1.853 μm), which they attributed to the $^3A_2 \rightarrow {}^3T_2$ transition of the V^{3+} ion. It remains unclear, however, if these lines belong to one or to both (h and k) sites. Further V^{3+}-related ZPL lines at around 7000 cm^{-1} have been attributed to higher excited states [32]. An apparently incomplete set of the V^{3+}-related ZPL has also been reported in 6H-SiC [32], where *two* ZPL at 4860 and 5002 cm^{-1} have to be associated with the *three* inequivalent V^{3+} centers. According to our DFT total energy calculations, also for the observed V^{3+}-related doublet in 4H-SiC, an attribution to a single defect appears to be more probable: clearly different ZPL energies for the lowest transitions are predicted for the h and k sites (PBEsol: 1.97 and 1.84 μm, respectively; cf. Table II). The nearly perfect agreement of the PBEsol-calculated $V^{3+}(k)$ ZPL with the experimental value might be surprising at first view. Nevertheless, we are dealing here with intra-3d shell transitions so that the usual underestimation of energy gaps and excitation energies calculated by semilocal functionals (see, e.g., also Refs. [18,20]) is relaxed (PBEsol) to some extent or, even overcompensated (PBE) by other effects, like spin contamination [47]. Interestingly and fully independent of the choice of the XC functional, the corresponding excited states for h, k are qualitatively different, since the order of the e and a_1 levels is inverted [see Fig. 3(b)]. Having this in mind, strongly different transition probabilities and by this a suppression of one of the two V^{3+}-related ZPL in 4H-SiC could be easily explained. Obviously, the assignment of the doublet line to either $V^{3+}(h)$ or $V^{3+}(k)$ requires further

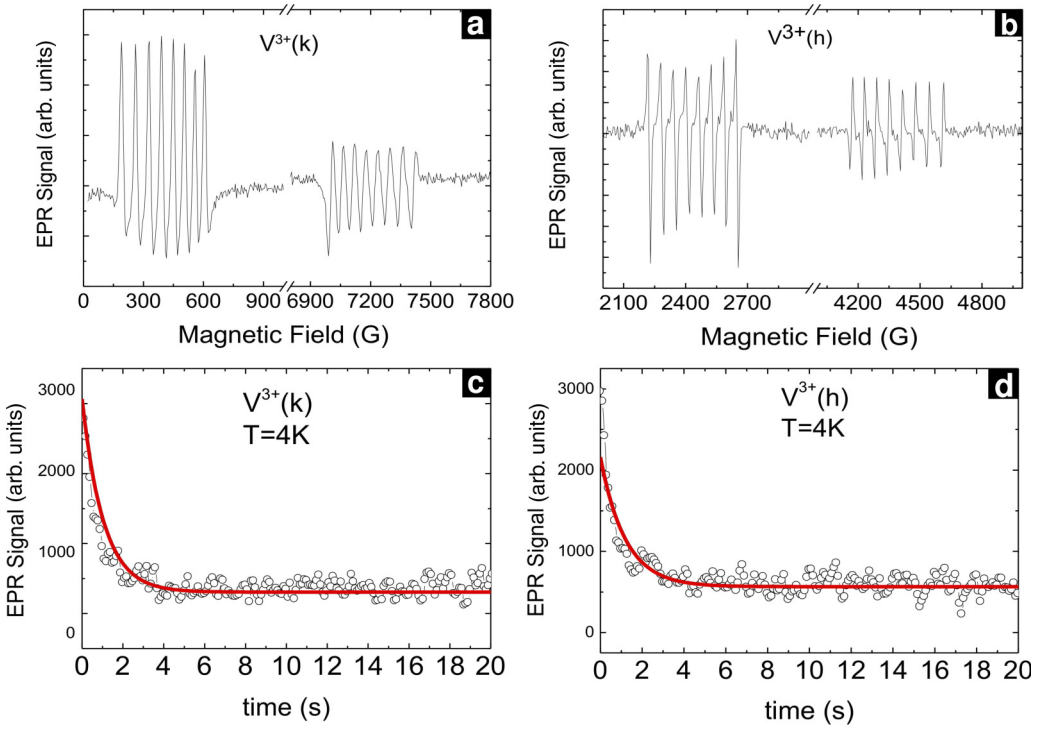

FIG. 4. (a) EPR spectrum of $V^{3+}(k)$ center under optical excitation, where $T = 4$ K and $\lambda = 1313$ nm. (b) EPR spectrum of $V^{3+}(h)$ center under optical excitation, where $T = 4$ K, $\lambda = 1313$ nm. (c) Time dependence of the ground-state spin polarization of the $V^{3+}(k)$ center at $T = 4$ K; (d) Time dependence of the ground-state spin polarization of the $V^{3+}(h)$ center at $T = 4$ K.

modeling (explicit calculation of transition probabilities) and, in particular, resonant excitation experiments [22], but tunable lasers in this wavelength range were not available in this study.

We have performed low-temperature photo-EPR measurements to investigate whether the ground-state spin distribution can be optically polarized. As shown in Figs. 4(a) and 4(b) the answer is yes; under photoexcitation in the near infrared (1.313 μm) the EPR spectra of both V^{3+} centers are strongly modified. As the ZPL emission lines from the first excited state are expected in the range of 1.8 μm [32], optical excitation at 1.3 μm is not unexpected. We observe a strong enhancement of the total intensity of the EPR spectra, and similar to the case of the NV^- centers, a phase inversion of the low-field and high-field $\Delta m_s = 1$ transitions. This is the fingerprint of an optically induced ground-state spin polarization [Figs. 2(b) and 2(c)], where due to spin selection rules the $m_s = 0$ level is predominantly populated. We observe a ground-state spin polarization of up to 70% under this nonresonant infrared excitation.

We have further investigated the spin-lattice relaxation time with which the ground-state spin polarization will relax back to its thermal equilibrium value. This information can be obtained by time-dependent cw-EPR, if the decay times are in the range of 100 ms or longer. This limit corresponds to the experimental limitations with which such measurements can be done by cw-EPR. We show in Figs. 4(c) and 4(d) the results obtained at $T = 4$ K. We observe for both centers a simple decay in the timescale of seconds. The decay can be fitted [see also Figs. 4(c) and 4(d)] with a single exponential decay function with a time constant T_1:

$$I(t) = I_0 \cdot \exp\left(-\frac{t}{T_1}\right) + A_0,$$

where we observe similar values of $T_1 = 0.6$ s and $T_1 = 0.8$ s for the $V^{3+}(k)$ and $V^{3+}(h)$ centers. It should be noted that this value of about 1 s is superior to the case of the intrinsic defects in SiC (NV, VV) and diamond (NV) investigated before.

V. CONCLUSION

In summary, we have investigated the magneto-optical properties of the hexagonal and quasicubic V^{3+} centers in 4*H*-SiC. Our combined experimental and theoretical study show that these centers fulfill all the basic requirements for application in quantum technology, shifting the optical spectral range still further in the infrared beyond 1.5 μm. Being single defects, not requiring interaction with intrinsic defects, their generation and spatial distribution should be easily controllable by ion implantation. Scalability should also be a minor problem due to the mature properties of 4*H*-SiC, a standard microelectronic material available in bulk and epitaxial layer form.

ACKNOWLEDGMENTS

S.A.Z. wishes to acknowledge support from the Quantum Nanophotonic Laboratory at Nanyang Technical University. W.B.G. would like to acknowledge the A*Star QTE program. U.G. and T.B. acknowledge support from the Deutsche Forschungsgemeinschaft (DFG) via priority program SPP 1601 (GE-1260/5-2).

[1] D. D. Awschalom, R. Hanson, J. Wrachtrup, and B. B. Zhou, Quantum technologies with optically interfaced solid-state spins, Nat. Photonics **12**, 516 (2018).

[2] M. Atatüre, D. Englund, N. Vamivakas, S. Y. Lee, and J. Wrachtrup, Material platforms for spin based photonic quantum technologies, Nat. Rev. Mater. **3**, 38 (2018).

[3] M. W. Doherty, N. B. Manson, P. Delaney, F. Jelezko, J. Wrachtrup, and L. C. L. Hollenberg, The nitrogen vacancy colour center in diamond, Phys. Rep. **528**, 1 (2013).

[4] P. Neumann, N. Mizuochi, F. Rempp, P. Hemmer, H. Watanabe, S. Yamasaki, V. Jacques, T. Gaebel, F. Jelezko, and J. Wrachtrup, Multipartite entanglement among single spins in diamond, Science **320**, 1326 (2008).

[5] G. D. Fuchs, G. Burkhard, P. V. Klimov, and D. D. Awschalom, A quantum memory intrinsic to single nitrogen-vacancy centers in diamond, Nat. Phys. **7**, 789 (2011).

[6] F. Jelezko, T. Gaebel, I. Popa, M. Domhan, A. Gruber, and J. Wrachtrup, Observation of Coherent Oscillation of a Single Nuclear Spin and Realization of a Two Bit Conditional Quantum Gate, Phys. Rev. Lett. **93**, 130501 (2004).

[7] J. R. Weber, W. F. Koehl, J. B. Varley, A. Janotti, B. B. Buckley, C. G. Van de Walle, and D. D. Awschalom, Quantum computing with defects, Proc. Natl. Acad. Sci. USA **107**, 8513 (2010).

[8] J. R. Weber, W. F. Koehl, J. B. Varley, A. Janotti, B. B. Buckley, C. G. Van de Walle, and D. D. Awschalom, Defects in SiC for quantum computing, J. Appl. Phys. **109**, 102417 (2011).

[9] A. Dzurak, Quantum computing: Diamond and silicon converge, Nature (London) **479**, 47 (2011).

[10] A. Boretti, Optical materials: Silicon carbide's quantum aspects, Nat. Photonics **8**, 88 (2014).

[11] L. Gordon, A. Janotti, and C. G. Van de Walle, Defects as qubits in 3*C*- and 4*H*-SiC, Phys. Rev. B **92**, 045208 (2015).

[12] D. Simin, H. Kraus, A. Sperlich, T. Oshima, G. V. Astakov, and V. Dyakonov, Locking of electronic spin coherence above 20 ms in in natural silicon carbide, Phys. Rev. B **95**, 161201(R) (2017).

[13] R. Nagy, M. Widmann, M. Niethammer, D. B. R. Dasari, I. Gerhardt, O. O. Soykal, M. Radulaski, T. Ohshima, J. Vuckovic, N. T. Son, I. G. Ivanov, S. E. Economou, C. Bonato, S. Y. Lee, and J. Wrachtrup, Quantum Properties of Dichroic Silicon Vacancies in Silicon Carbide, Phys. Rev. Appl. **9**, 034022 (2018).

[14] M. Widmann, S. Y. Lee, T. Rendler, N. T. Son, H. Fedder, S. Paik, L.-P. Yang, N. Zhao, S. Yang, I. Booker, A. Denisenko, M. Jamali, S. A. Momenzadeh, I. Gerhardt, T. Oshima, A. Gali, E. Janzén, and J. Wrachtrup, Coherent control of single spins in silicon carbide at room temperature, Nat. Mater. **14**, 164 (2014).

[15] A. L. Falk, P. V. Klimov, V. Ivady, K. Szasz, D. J. Christle, W. F. Koehl, A. Gali, and D. D. Awschalom, Optical Polarization of Nuclear Spins in Silicon Carbide, Phys. Rev. Lett. **114**, 247603 (2015).

[16] D. J. Christle, A. L. Falk, P. Andrich, P. V. Klimov, J. Ul Hassan, N. T. Son, E. Janzen, T. Oshima, and D. D. Awschalom, Isolated electron spins in silicon carbide with millisecond coherence times, Nat. Mater. **14**, 160 (2015).

[17] H. J. von Bardeleben, J. L. Cantin, E. Rauls, and U. Gerstmann, Identification and magneto-optical properties of the NV center in 4*H*-SiC, Phys. Rev. B **92**, 064104 (2015).

[18] H. J. von Bardeleben, J. L. Cantin, A. Csóré, A. Gali, E. Rauls, and U. Gerstmann, NV centers in 3C, 4*H*, and 6*H* silicon carbide: A novel platform for solid-state qubits and nanosensors, Phys. Rev. B **94**, 121202(R) (2016).

[19] H. J. von Bardeleben and J. L. Cantin, NV centers in silicon carbide: From theoretical predictions to experimental observation, MRS Commun. Res. Lett. **7**, 591 (2017).

[20] A. Csóré, H. J. von Bardeleben, J. L. Cantin, and A. Gali, Characterization and formation of NV centers in 3C, 4*H*, and 6HsiC: An *ab initio* study, Phys. Rev. B **96**, 085204 (2017).

[21] S. A. Zargaleh, S. Hameau, B. Eble, F. Margaillan, H. J. von Bardeleben, J. L. Cantin, and W. Gao, Nitrogen vacancy center in cubic silicon carbide: A promising qubit in the 1.5 μm spectral range for photonic quantum networks, Phys. Rev. B **98**, 165203 (2018).

[22] S. A. Zargaleh, H. J. von Bardeleben, J. L. Cantin, U. Gerstmann, S. Hameau, B. Eble, and W. Gao, Electron paramagnetic resonance tagged high-resolution excitation spectroscopy of NV- centers in 4*H*-SiC, Phys. Rev. B **98**, 214113 (2018).

[23] T. Bosma, G. J. J. Lof, C. M. Gilardoni, O. V. Zwier, F. Hendriks, B. Magnusson, A. Ellison, A. Gallstrom, I. G. Ivanov, N. T. Son, R. W. Havenith, and C. H. van der Walle, Identification and tunable optical control of transition-metal spins in silicon carbide, npj Quantum Inf. **4**, 48 (2018).

[24] A. Lohrmann, A. Csoré, G. Thiering, S. Putz, R. Karhu, J. Ul Hassan, N. T. Son, T. Fromherz, A. Gali, and M. Trupke, A review on single photon sources in silicon carbide, Rep. Prog. Phys. **80**, 034502 (2017).

[25] L. Spindlberger, A. Csoré, G. Thiering, S. Putz, R. Karhu, J. Ul Hassan, N. T. Son, T. Fromherz, A. Gali, and M. Trupke, Optical Properties of Vanadium in 4*H* Silicon Carbide for Quantum Technology, Phys. Rev. Appl. **12**, 014015 (2019).

[26] Y. Zhang, C. Wang, Y. Zhang, Y. Wang, H. Gao, X. Tang, and H. Lu, *Semi-insulating SiC formed by Vanadium implantation, IEEE International Conference on Electron Devices and Solid-State Circuits* (IEEE, New York, 2008), pp. 1–6.

[27] W. C. Mitchel and W. D. Mitchell, Vanadium donor and acceptor levels in semi-insulating 4*H*-and 6*H*-SiC, J. Appl. Phys. **101**, 013707 (2007).

[28] J. R. Jenny, J. Skowronski, W. C. Mitchel, H. M. Hobgood, R. C. Glass, G. Augustine, and R. H. Hopkins, DLTS and Hall effect investigation of the position of the acceptor level in 4H-SiC, Appl. Phys. Lett. **68**, 1963 (1996).

[29] M. Kunzer, U. Kaufmann, K. Maier, and J. Schneider, Magnetic circular dichroism and electron spin resonance of the A-acceptor state of vanadium,V^{3+}in 6H-SiC, Mater. Sci. Eng. B **29**, 118 (1995).

[30] J. Schneider, H. D. Müller, K. Maier, W. Wilkening, F. Fuchs, A. Dörnen, S. Leibenzeder, and R. Stein, Infrared spectra end electron spin resonance of vanadium deep level impurities in silicon carbide, Appl. Phys. Lett. **56**, 1184 (1990).

[31] P. Kaminska, High resolution photoinduced transient spectroscopy of deep centers in vanadium doped semi-insulating SiC, J. Mater. Sci: Mater. Electron **19**, 224 (2008).

[32] V. Lauer, G. Bremond, A. Souifi, G. Guillot, K. Chourou, M. Anikin, R. Madar, B. Clerjeaud, and C. Naud, Electrical and optical characterization of vanadium in 4H-and 6H-SiC, Mater. Sci. Eng. B **61**, 248 (1999).

[33] V. Ivády, J. Davidsson, N. T. Son, T. Ohshima, I. A. Abrikosov, and A. Gali, Identification of Si-vacancy related

room-temperature qubits in 4*H* silicon carbide, Phys. Rev. B **96**, 161114(R) (2017).

[34] A. L. Falk, B. B. Buckley, G. Calusine, W. F. Koehl, V. V. Dobrovitski, A. Politi, C. A. Zorman, P. X.-L. Feng, and D. D. Awschalom, Polytype control of spin qubits in silicon carbide, Nat. Commun. **4**, 1819 (2013).

[35] P. Giannozzi *et al.*, Quantum ESPRESSO: A modular and open-source software project for quantum simulations of materials, J. Phys.: Condens. Matter **21**, 395502 (2009).

[36] P. Giannozzi *et al.*, Advanced capabilities for materials modeling with Quantum ESPRESSO, J. Phys. Condens. Matter **29**, 465901 (2017).

[37] T. Biktagirov, W. G. Schmidt, and U. Gerstmann, Calculation of spin-spin zero-field splitting within periodic boundary conditions: Towards all-electron accuracy, Phys. Rev. B **97**, 115135 (2018).

[38] T. Biktagirov, W. G. Schmidt, and U. Gerstmann, Efficient scheme to eliminate spin contamination in magnetic dipolar coupling: Rectifying the zero field splitting of NV^- centers, arXiv:1909.13577.

[39] J. P. Perdew, K. Burke, and M. Ernzerhof, Generalized Gradient Approximation Made Simple, Phys. Rev. Lett. **77**, 3865 (1996).

[40] R. Armiento and A. E. Mattsson, Functional designed to include surface effects in self-consistent density functional theory, Phys. Rev. B **72**, 085108 (2005).

[41] V. Grachev, Visual EPR simulation tool, University of Montana, www.visual-epr.com.

[42] T. Biktagirov, W. G. Schmidt, U. Gerstmann, B. Yavkin, S. Orlinskii, P. Baranov, V. Dyakonov, and V. Soltamov, Polytypism driven zero-field splitting of silicon vacancies in 6*H*-SiC, Phys. Rev. B **98**, 195204 (2018).

[43] P. Neumann, I. Jacobi, F. Dolde, C. Burk, R. Reuter, G. Waldherr, J. Jonert, T. Wolf, A. Brunner, J. H. Shim, D. Suter, H. Sumiya, J. Isoya, and J. Wrachtrup, High-precision nanoscale temperature sensing using single defects in diamond, Nano Lett. **13**, 2738 (2013).

[44] H. Kraus, V. A. Soltamov, F. Fuchs, D. Simin, A. Sperlich, P. G. Baranov, G. V. Astakhov, and V. Dyakonov, Magnetic field and temperature sensing with atomic-scale spin defects in silicon carbide, Sci. Rep. **4**, 5303 (2014).

[45] M. W. Doherty, V. M. Acosta, A. Jarmola, M. S. J. Barson, N. B. Manson, D. Budker, and L. C. L. Hollenberg, Temperature shifts of the resonances of the NV center in diamond, Phys. Rev. B **90**, 041201(R) (2014).

[46] D. Prezzi, T. A. G. Eberlein, J. S. Filhol, R. Jones, M. J. Shaw, P. R. Briddon, and S. Öberg, Optical and electrical properties of vanadium and erbium in 4*H*-SiC, Phys. Rev. B **69**, 193202 (2004).

[47] A. Ipatov, F. Cordova, L. J. Doriol, and M. E. Casida, Excited-state spin-contamination in time-dependent density-functional theory for molecules with open-shell ground states, J. Mol. Struct.: THEOCHEM **914**, 60 (2009).